



Nanovaccine impact on dendritic cells: transcriptome analysis enables new insights into antigen and adjuvant effects

David Paßlick^{‡,1,2}, Jonas Reinholz^{‡,1,2}, Johanna Simon^{1,2}, Keti Piradashvili², Shuai Jiang², Mengyi Li², Katharina Landfester²  & Volker Mailänder^{*,1,2} 

¹Dermatology Clinic, University Medical Center Mainz, Langenbeckstraße 1, Mainz, 55131, Germany

²Physical Chemistry of Polymers, Max Planck Institute for Polymer Research, Ackermannweg 10, Mainz, 55128, Germany

*Author for correspondence: mailaend@mpip-mainz.mpg.de

‡Authors contributed equally

Aim: For vaccines the combination between an antigen and adjuvants are both crucially important to trigger an effective immune response in dendritic cells. Innovative adjuvants like resiquimod or muramyl dipeptide have their target protein inside the cell. **Materials & methods:** Up/downregulation and proteome expression was investigated for the adjuvant combination resiquimod and muramyl dipeptide in a soluble form versus encapsulated into a nanocarrier. **Results:** We found that 1225 genes were upregulated after nanocarrier treatment while 478 genes were downregulated. Most prominent were interferon-stimulated genes with more than 25-times higher expression after nanocarrier treatment, for example *RSAD2* and *ISG15*, which were recently found to have antiviral or antitumor effects. **Conclusion:** Encapsulation gives a more effective upregulation of vaccine-related genes.

First draft submitted: 22 December 2019; Accepted for publication: 10 June 2020; Published online: 4 September 2020

Keywords: adjuvants • downregulation • interferon-related genes • nanocapsule • proteomics • RNAseq • stimulation • upregulation • vaccine

Even today, the cellular processes triggered by a vaccine leading to the well-known long-term protection are highly complex and not completely deciphered. Antigen and adjuvants are co-administered as two components. Each component is recognized independently and evokes distinct effects in the associated cell or tissue. Dendritic cells (DCs) are the key players for taking up and processing vaccine components. The recognition of the adjuvant via specific receptors activates the DCs, while the antigen is intracellularly processed and thereafter, presented to the surrounding cells. The combined effect of both components in the DC is essential for a successful vaccination. Both components are commonly not coupled chemically nor physically. While some of the adjuvants are recognized by cell surface receptors, others need to get into the endosome or the cytoplasm of the cell. After injection, they diffuse independently from each other through the tissue and need to reach and cross into the DC independently. In contrast, the application of vaccines via a nanoparticulate formulation, for instance a nanocapsule (NC), enables a coupled delivery of antigen and adjuvant into the same target cell. The NC uptake mediates the delivery of both components. While the antigen always needs to be endocytosed, some of the more interesting adjuvants also have an intracellular target receptor. Moreover, NCs offer the potential to add diverse chemical modifications, for instance for DC targeting. While a lot of work has been done to compare the effects of common (soluble) versus encapsulated vaccines, the transcriptome, in other words the complete mRNA expression profile of such treated DCs was rarely taken into account to understand the actual impact of encapsulated vaccine.

In this study, we used ovalbumin (OVA)-based NCs (OVA-NCs) with an aqueous core as delivery system as well as antigen source to treat murine bone marrow-derived DCs (BMDCs). In previous studies, the uptake kinetics and the controlled payload release of these OVA-NCs have already been investigated in murine [1] and human [2] DCs. Additionally, these capsules (OVA-Adj-NCs) have already been loaded with the adjuvant combination muramyl dipeptide (MDP) and resiquimod (R848) and used as nanovaccine. It was shown that DC treatment with

OVA-Adj-NCs induced a synergistic DC activation and thus an effective T-cell stimulation [1]. Additionally, it was proven that the NCs were more efficient than the soluble application of the respective components in equimolar amounts. In literature, there is limited information about the overall transcriptional effects of specific adjuvants or delivery systems. With some exceptions, such as protamine–RNA complexes, CpG-P [3], or heparan sulfate [4], the transcriptional adjuvant effect is rarely in the focus of vaccination studies. At least, soluble R848 was shown to trigger an increased mRNA expression of IL-6, IL-12 α and IL-12 β upon BMDC stimulation for 4 h [5]. Moreover, transcriptional changes in BMDCs treated with E2 and fd filamentous bacteriophages, two promising delivery systems, were also investigated [6].

Here, we analyzed the transcriptome of BMDCs incubated with OVA-Adj-NCs by RNA-Seq. In this way, we were able to determine mRNA expression patterns characterizing the combined delivery of an antigen and adjuvants via a nanocarrier. These data provide insight into the immunological properties of nanocarriers used for vaccination. Additionally, it gives a deeper understanding about the differences for a nanocarrier based vaccine delivery system in comparison with a soluble vaccination approach. Moreover, proteomic analysis gave additional information about the cellular processes after nanocarrier treatment. At last, this is the first study, which analyzes the transcriptome of BMDCs with RNA-Seq. Although many literature reports investigated BMDCs in immunological studies, only gene microarray or quantitative polymerase chain reaction (qPCR) analyses were performed for selected genes [7,8].

Materials & methods

Synthesis of OVA NCs

As previously described OVA-NCs were synthesized in the same procedure and therefore the method can also be found in [1]. We sum up the method here again: In 500 μ l sterile, deionized water 50 mg OVA (grade VI, Sigma-Aldrich, Deisenhofen, Germany) was dissolved with 7.14 mg NaCl. To this aqueous phase, 13 nmol Cy5-labeled oligonucleotides (cyanine5-5'- CCA CTC CTT TCC AGA AAA CT, IBA GmbH, Göttingen, Germany) were added. Afterward 35.8 mg of the surfactant P([E/B]-b-EO) were dissolved in 7.5 g of cyclohexane (VWR, PA, USA). P([E/B]-b-EO) consists of a poly(ethylene-co-butylene) block and a poly(ethylene oxide) block [9]. Under stirring, we then added this to the aqueous phase. The pre-emulsion was homogenized by ultrasonication. In a separate vial, 10.7 mg P([E/B]-b-EO) were dissolved in 5 g of cyclohexane and 2 mg 2,4-toluene diisocyanate (Sigma-Aldrich). This mixture was then added dropwise to the obtained mini-emulsion. The reaction was allowed to proceed for 24 h at 25°C. The samples were further processed by repetitive centrifugation and replacement of the supernatant with fresh cyclohexane. This removed the excess surfactant from the obtained NCs. Six hundred microliters of the dispersion from cyclohexane were added dropwise to 5 ml of a 0.1 wt-% aqueous SDS (Alfa Aesar, Heysham, UK) solution. By this the NC were transferred to water. During transfer the aqueous solution was placed in an ultrasound bath. In order to evaporate cyclohexane the sample was stirred with an open cap overnight. Via four centrifugation steps and replacing the supernatant with sterile, deionized water excess SDS was removed. R848 and MDP (Invivogen, Toulouse, France), 70 μ l R848 (10 mg/ml in DMSO) and 250 μ l MDP (10 mg/ml in water) were encapsulated in the respective preparations as indicated. In order to maintain 500 μ l of total volume, the amount of water was reduced to end up with the same endvolume. The ultrasonication device was a Branson Sonifier W-450-Digital (CT, USA) equipped with a microtip. Sonication parameters were as followed: 3 min at 70% amplitude with a pulse of 20 s sonication and 10 s pauses in between. By dynamic light scattering, we determined the average size and size distribution of the NCs. The measurements were done at 25°C with a Nicomp 380 submicron particle sizer (Nicomp Particle Sizing Systems, FL, USA) measuring at fixed angle of 90°. ζ potential was done in 10⁻³ M potassium chloride solution at pH 6.8 and 25°C by using a Malvern Zeta sizer (Malvern Instruments, Herrenberg, Germany). Before usage, all OVA-NC batches were analyzed for endotoxin contamination by limulus amoebocyte lysate assay (Thermo Fisher Scientific, MA, USA) according to the manufacturer's instructions. Based on the US FDA's 'Guidance for Industry: Pyrogen and Endotoxin Testing,' the endotoxin limit was to set 0.5 EU/ml. OVA-NC batches with higher endotoxin concentrations were not used for cellular experiments.

Quantification of encapsulated MDP & R848

As previously described the content of the NCs concerning MDP and R848 were analyzed with the same procedure as published before and therefore the method can also be found in [1]. We sum up the method here again: with a centrifugal filter with molecular weight cutoff of 100 kDa (Merck Millipore, Darmstadt, Germany), the supernatants of the NC dispersions were separated from the capsules themselves. The pellet was redispersed in

phosphate-buffered saline (PBS) containing 2 mg/ml of trypsin. These were incubated for 24 h. The absorbance at $\lambda = 325$ nm for R848 was used to determine the concentration of R848. This was done on a Lambda 16 UV-Vis spectrometer (Perkin Elmer, MA, USA). A calibration curve in the range of 0.01–1 mg/ml was used to determine the concentration of R848. As MDP has no characteristic adsorbance, we needed to use modified MDP by an Alexa Fluor 488 5-SDP ester. This was done following the manufacturer's instructions (Thermo Fisher Scientific). The amount of MDP-Alexa 488 was determined by using a plate reader (Excitation 498 nm, Emission 519 nm). The calibration curve was determined in a range of 0.34–2.26 μg .

Mice

C57BL/6 mice were bred and maintained in the Translational Animal Research Center of the University Medical Center Mainz under pathogen-free conditions on a standard diet. The recommendations of the Guide for the Care and Use of Laboratory Animals by the National Institutes of Health were followed.

Generation of murine BMDCs

BMDCs were differentiated from bone marrow progenitors of 8–10-week-old C57BL/6 mice as described by Bros *et al.* [10]. Under sterile conditions, iliac crests, femora and tibiae were prepared from C57BL/6 mice, cleaned with 70% ethanol and transferred to IMDM containing 5% fetal calf serum (FCS) (both from Sigma-Aldrich) and 50 μM β -mercaptoethanol (Roth, Karlsruhe, Germany). Bones were sliced and rinsed with a small cannula to wash out the bone marrow. Bone marrow cells were separated with a 40- μm cell strainer (Greiner Bio-One, Frickenhausen, Germany) and centrifuged for 10 min at 4°C and 300 $\times g$. Then, 2×10^6 cells were transferred to a petri dish in 10 ml IMDM containing 2 mM L-glutamine, 100 U/ml penicillin, 100 $\mu\text{g}/\text{ml}$ streptomycin (all from Sigma-Aldrich) and 50 μM 2-mercaptoethanol, supplemented with 5% GM-CSF containing cell culture supernatant derived from X63.Ag8-653 myeloma cells stably transfected with a murine GM-CSF expression construct [11]. After 3 and 6 days, respectively, 5 ml medium containing GM-CSF was added to the petri dish. On day 7 or 8, nonadherent DCs were harvested by gentle rinsing. Cells were transferred to six-well plates for further experiments.

DC treatment with adjuvants/NCs

A total of 2×10^6 BMDCs/well were seeded into six-well plates in 1 ml IMDM containing 2 mM L-glutamine, 5% FCS, 100 U/ml penicillin, 100 $\mu\text{g}/\text{ml}$ streptomycin and 50 μM β -mercaptoethanol as well as GM-CSF as mentioned before. The next day, cells were treated with 75 $\mu\text{g}/\text{ml}$ NCs. Here, either OVA NCs loaded with both R848 and MDP, or empty OVA NCs as control were added to the cells for 1, 2 and 4 h. For comparison, further BMDC samples were treated with soluble R848 (83.25 ng/ml) and MDP (287.25 ng/ml) in concentrations equimolar to encapsulated adjuvants, also for 1, 2 and 4 h. One set of BMDCs was left untreated as a negative control reference. Each treatment was carried out in duplicates. Afterward, samples of the different time points were pooled and total RNA was extracted via RNeasy Mini Kit (Qiagen, Hilden, Germany) according to the manufacturer's recommendations. RNA quality was analyzed via agarose gel electrophoresis and Bioanalyzer (Agilent Technologies, CA, USA). RNA quantity was determined via NanoDrop 8000 spectrophotometer (Thermo Fisher Scientific). Afterward, total RNA was handed over to StarSeq (Mainz, Germany) for subsequent Illumina Next Generation Sequencing.

Illumina sequencing

cDNA library preparation and Illumina Next Generation Sequencing were carried out by StarSeq. Thereafter, mRNAs were sequenced via Illumina NextSeq 500™ (Illumina, CA, USA). Overall, at least 25 million paired-end reads were created per sample (2×150 nt, 3.75 Gb) for the eight datasets (two untreated samples, two samples treated with empty OVA-NCs, two samples treated with MDP/R848-loaded OVA-NCs, two samples treated with soluble MDP/R848). Data were received in .fastq format.

Quantification of RNA-seq datasets

Obtained next-generation sequencing (NGS) datasets were quantified using the software Geneious R8 (Biomatters, New Zealand). First, NGS files were imported in .fastq format. Then, paired-end reads were assigned to each other, whereat the distance was set to 470 bp. The annotated genomic murine reference sequence was obtained by NCBI (GFF_GCF.000001635.25_GRCm38.p_genomic.gff) and imported into the software. Finally, all datasets were

mapped against the murine reference sequence. For this purpose, all 21 annotated murine chromosomes as well as the annotated murine mitochondrial DNA were used as reference sequences for the mapping to create contigs and for contigs quantification by using the Geneious R8 function 'Calculate expression levels' by using defined parameters (Supplementary Table 1).

Then, expression data were transferred to an MS Excel sheet and differences in gene expression were quantified using the transcripts per kilobase million (TPM) values. Finally, also the ratios of TPM values of the different sample conditions were calculated (whereat the negative control was set as '1'). These ratios were subsequently used to visualize expression differences via heat maps and scatter plots.

Quantitative PCR

All cDNAs for qPCR were synthesized with the iScript™ cDNA Synthesis Kit (Bio-Rad, CA, USA) according to the manufacturer's protocol. Standard 20 µl cDNA synthesis consisted of the components 5X iScript Reaction Mix (4 µl), iScript Reverse Transcriptase (1 µl), the RNA template (1–100 ng) and nuclease-free water (to 20 µl). cDNA reactions were briefly mixed by pipetting up and down and then transferred to the Mastercycler EP Gradient S (Eppendorf, Germany) for cDNA synthesis (Supplementary Table 2). For quantitative real time PCRs, specific qPCR primers (Supplementary Table 3) were designed for the amplification of approximately 200 bp DNA fragments.

Standard 20 µl amplification reaction consisted of the components iQ SYBR Green Supermix (10 µl), F-Primer (1 µl), R-Primer (1 µl), cDNA template (3 ng) and nuclease-free water (to 20 µl). All ingredients were mixed gently by pipetting up and down and then transferred to the real time system CFX96 (Bio-Rad) for cyclic amplification and measurement of SYBR Green dye (Supplementary Table 4). Finally, gene expression was calculated by using the $\Delta\Delta C_t$ -method [12]. GAPDH was used as a reference gene. The melt curve was analyzed manually for successful amplification of target DNA fragments.

Liquid chromatography coupled to mass spectrometry

Protein extraction and digestion was carried out as previously published [13,14]. Briefly, cells were dissolved in lysis buffer containing 7 M urea, 2 M thiourea, 2% CHAPS and incubated for 15 min at 37°C and centrifuged for 1 h (4°C 20.000×g). Further, the supernatant was transferred into a 1.5 ml protease-free tubes and the protein concentration was determined by Pierce™ 660 nm Protein Assay Kit (Thermo Fisher Scientific) according to the manufactures' instructions.

Extracted proteins were precipitated overnight using ProteoExtract protein precipitation kit (Cal-BioChem, Darmstadt, Germany) according to the manufactures' instructions and resuspend in RapiGest SF (Waters Cooperation, Eschborn, Germany) dissolved in ammonium bicarbonate (50 mM) buffer. Samples were incubated at 80°C for 15 min, reduced with dithiothreitol (Sigma-Aldrich, 5 mM, 45 min, 56°C) and alkylated with iodoacetamide (Sigma, 15 mM, 1 h, room temperature [RT]). For digestion a protein: trypsin ratio of 50:1 over 16 h at 37°C was used. The reaction was quenched hydrochloric acid (Sigma).

Peptide samples were diluted with 0.1% formic acid and spiked with 50 fmol µl⁻¹ Hi3 Ecoli (Waters Cooperation) standard for absolute protein quantification [15]. Proteomic measurements were performed with a nanoACQUITY UPLC system coupled with a Synapt G2-Si mass spectrometer. A NanoLockSpray source was used for electrospray ionization in positive ion mode and the Synapt G2-Si was operated in resolution mode. Data were acquired and processed with MassLynx 4.1 was used. Proteins were identified with Progenesis QI (2.0) using a reviewed human data base (Uniprot). Processing parameters were set as described in previous reports [16,17]. The amount of each protein was determined in fmol based on the TOP3/Hi3 approach [18].

Results

NC characterization

All OVA-NC formulations were produced in inverse mini-emulsion using cyclohexane as continuous phase [2]. After purification and transfer of the OVA-NCs into water, cyclohexane was efficiently removed as shown by ¹H-NMR measurements (Supplementary Figure 1). The diameter of the empty OVA-NCs was determined to be 256 nm in cyclohexane and 348 nm after transfer into water. Their ζ potential was -26 mV. The adjuvant-loaded OVA-NCs showed a diameter of 302 nm in cyclohexane, 338 nm in water and a ζ potential of -31 mV (Supplementary Table 5) Diameters of the experimentally used OVA-NCs in cyclohexane and water as well as the ζ potential were measured via dynamic light scattering. Data were previously shown in [1]. Encapsulated MDP and

R848 were measured via fluorescence spectroscopy. Adjuvant loading was determined to be 7.14 nmol MDP (with an encapsulation efficiency of 73.6%) and 2.85 nmol R848 (with an encapsulation efficiency of 65.9%) per mg NC (Supplementary Table 6). Characterization of the used OVA-NCs (\pm adjuvants) has already been described in a previous publication [1].

Besides all this, the adjuvant loading capacities of OVA-NCs and the resulting encapsulation efficiencies were measured and calculated to determine the amount of MDP and R848 per mg OVA-NC, and to be able to analyze how much adjuvant is actually available during cellular treatment. It turned out that MDP showed higher encapsulation efficiency in OVA-NCs than R848, most likely due to its better solubility characteristics in water. In the end, the loading capacity of the OVA-NCs and therefore the encapsulation efficiencies of each adjuvant is determined and limited by the underlying manufacturing process.

RNA extraction of differently treated DCs

BMDCs were treated with 75 $\mu\text{g}/\text{ml}$ OVA-NCs, either empty or loaded with adjuvants, or equimolar amounts of soluble adjuvants for 1, 2 and 4 h. Afterward, the respective wells containing different time points of incubations were pooled together prior to RNA extraction to ensure to not miss the optimal time point of transcriptomic changes after the NC/adjuvant treatment. This was performed for two sets of BMDCs = two biological replicates for each treatment. Finally, total RNA was extracted, and quality controlled via Bioanalyzer measurements, a device that provides automated electrophoretic separations. The Bioanalyzer software calculates the RNA Integrity Number, which is based on the intensity ratios of the 28S rRNA, 18S rRNA and the background signal [19]. Total extracted RNA was around 100–300 ng/ μl for each sample (Supplementary Figures 2–9). All RNA samples featured RNA Integrity Number values of at least 9.4, indicating a high quality. After confirming sufficient quality, RNA samples were transferred to StarSeq (Mainz, Germany) for mRNA extraction, cDNA library creation, and Illumina sequencing. By this procedure, a total of 25 million reads with each 150 nucleotides per sample were obtained in .fastq format, which represents genetic information of >3.7 gb of DNA per sample. All samples were mapped against the 21 annotated murine chromosomes as well as the annotated murine mitochondrial DNA sequence. A total number of 76,640 transcripts were detected, corresponding to 22,558 murine genes, which fits the number of protein-coding genes described in literature [20]. All genes were finally analyzed for their TPM values. Genes which did not exhibit a TPM value of at least 20 in two or more samples were removed. For the 10,135 remaining genes, we calculated the mean values of the two biological replicates and thus the relative expression ratios in the NCs-treated samples (\pm adjuvants) against the untreated control.

Expression of relevant gene groups

The transcriptome of BMDCs treated with 75 $\mu\text{g}/\text{ml}$ OVA-Adj-NCs or equimolar amounts of soluble adjuvants (1, 2 and 4 h pooled) were analyzed by RNA-Seq. As a control we used untreated BMDCs as well as BMDCs treated with empty OVA-NCs. Transcriptome analysis allows a deeper understanding of the cellular processes that were initiated by a nanocarrier and its payload. Moreover, we analyzed the differences between soluble and encapsulated adjuvant delivery.

First of all, the generated gene list was scanned for genes, which could be assigned to defined categories of interest (Supplementary Box 1). The TPM values of the corresponding genes were used to be able to determine the general expression level of each gene and to perform a preselection. Furthermore, the relative expression ratios against the untreated control were analyzed comparatively to identify changes on RNA level triggered by the empty OVA-NCs, OVA-Adj-NCs or the corresponding soluble adjuvant combination.

Prominent upregulation of interferon-stimulated genes by encapsulated adjuvants

The most prominent differences between soluble and encapsulated adjuvant application on mRNA level were detectable for the group of interferon (IFN)-stimulated genes (ISGs), which are usually triggered by Type I IFNs [21]. Numerous of those mRNAs were strongly upregulated by OVA-Adj-NCs, whereas the soluble adjuvant treatment as well as the incubation with empty OVA-NC did not evoke such a tremendous effect. By OVA-Adj-NC treatment many genes were upregulated by more than 25–30-fold compared with the untreated control. ISGs, such as *RSAD2* and *ISG15*, were especially prominent. Moreover, both ISGs have already been described to be beneficial for an effective antitumor immune response. *RSAD2* has been reported as a necessary factor for DC maturation in a B16F10 pulmonary metastasis model [22], while *ISG15* has been identified to trigger antitumor immune responses by promoting intratumoral infiltration of natural killer (NK) cells and enhancing antigen presentation

Interferon-stimulated genes				
Gene	Untreated	OVA-NCs	Sol. Adj	OVA-Adj-NCs
<i>IFIT3</i>	1,0	7,3	2,6	57,1
<i>IFIT3B</i>	1,0	6,3	4,6	49,0
<i>IFIT1BL1</i>	1,0	13,0	4,6	47,0
<i>IFI44</i>	1,0	4,0	1,8	44,3
<i>IFIT2</i>	1,0	5,1	4,6	35,7
<i>IFIT1</i>	1,0	5,3	5,2	33,5
<i>RSAD2</i>	1,0	4,5	3,3	32,5
<i>ISG15</i>	1,0	3,6	3,3	27,1
<i>IFI205</i>	1,0	3,5	7,9	18,9
<i>OASL1</i>	1,0	4,8	3,7	22,4
<i>CMPK2</i>	1,0	2,7	2,6	13,4
<i>OASL2</i>	1,0	2,8	1,7	13,2
<i>OAS3</i>	1,0	2,6	1,5	11,1
<i>TGTP1</i>	1,0	2,2	4,7	6,7
<i>IFI204</i>	1,0	1,8	2,0	8,8
<i>IFI203</i>	1,0	1,9	5,7	4,9
<i>ISG20</i>	1,0	2,7	1,4	8,9
<i>TGTP2</i>	1,0	1,9	2,4	7,3
<i>IFI47</i>	1,0	1,7	2,0	6,2
<i>OAS2</i>	1,0	2,2	1,0	6,6
<i>USP18</i>	1,0	1,7	2,5	4,1
<i>OAS1G</i>	1,0	1,6	1,4	4,3
<i>IFIH1</i>	1,0	1,5	1,7	4,0
<i>OAS1A</i>	1,0	1,5	1,3	3,8
<i>IFI27L2A</i>	1,0	1,6	0,9	2,6
<i>OAS1C</i>	1,0	1,2	1,2	1,8
<i>IFI35</i>	1,0	1,2	1,1	1,7
<i>IFI27</i>	1,0	1,2	1,1	1,0
<i>IFI30</i>	1,0	1,2	0,9	1,1

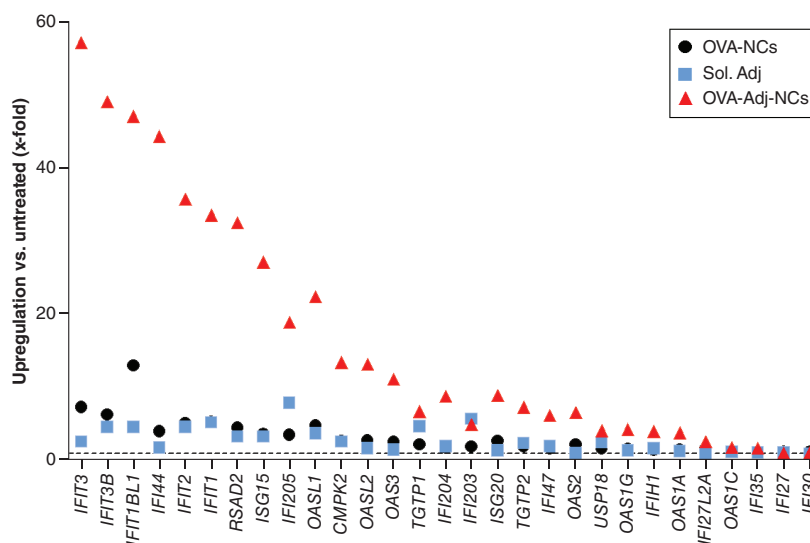


Figure 1. mRNA expression ratios of interferon-stimulated genes. The relative mRNA expression ratios of diverse IFN-stimulated genes of bone marrow-derived dendritic cells (2×10^6 cells/ml) treated with empty OVA-NCs, OVA-Adj-NCs (both 75 $\mu\text{g/ml}$), or equimolar amounts of soluble adjuvants were calculated against the untreated control. Dashed line indicates mRNA expression of untreated control. Tests were performed in duplicate ($n = 2$). NC: Nanocapsule; OVA: Ovalbumin.

in tumor cells 25. With some exceptions, such as *IFIT3*, *IFIT3B* and *IFIT1BL1* for empty OVA-NCs and *IFI205* for soluble MDP/R848, the effect of these two treatments on ISG expression was generally rather weak (Figure 1). These results indicated that an ISG upregulation is highly dependent on the combined presence of OVA-NC (representing the antigen) and the adjuvants. Although BMDC stimulation with soluble MDP/R848 triggered a strong transcriptional upregulation of costimulatory molecules and pro-inflammatory cytokines (see Figure 2A & 3), it was not sufficient to mediate Type I IFN-dependent ISG upregulation. A highly increased mRNA expression of *IRF7* upon treatment with OVA-Adj-NCs, but noticeably weaker with empty OVA-NC or equimolar amounts of soluble adjuvants (Supplementary Figure 10) underlines our results, since *IRF7* is a crucial regulator of Type I IFNs in pathogenic infections [23].

Up/downregulation of costimulatory & DC markers

Costimulation is a major requirement for an adaptive DC-mediated immune reaction. Focusing on the corresponding genes in BMDCs, we observed an increased expression for *CD40*, *CD80*, *CD83* and *CD86* mRNA as well as for *TNFSF4 (OX40L)* and *ICAM1* after treatment with MDP/R848-loaded OVA-NCs compared with the untreated control and those treated with empty OVA-NCs. In case of equimolar amounts of soluble adjuvants, the expression of only *CD40* and *ICAM1* were noticeably influenced. The further costimulatory marker mRNAs of this treatment showed expression levels similar to those of the empty OVA-NC sample (Figure 2A). These results were consistent with our previous measurements of costimulatory molecule expression on protein level upon treatment with OVA-Adj-NCs [1]. In this case, the encapsulated delivery of MDP and R848 via OVA-NCs enhanced their stimulatory potential to trigger mRNA expression of costimulatory molecules in BMDCs compared with the soluble application.

In contrast, the NC or the soluble adjuvant treatment did not influence the expression of typical DC marker genes such as *ITGAX (CD11c)*. Compared with the untreated control, the expression of *ITGAX (CD11c)* and *ITGAM (CD11b)* was actually decreased upon incubation with OVA-MDP/R848-NCs (Figure 2B). Downregulation of

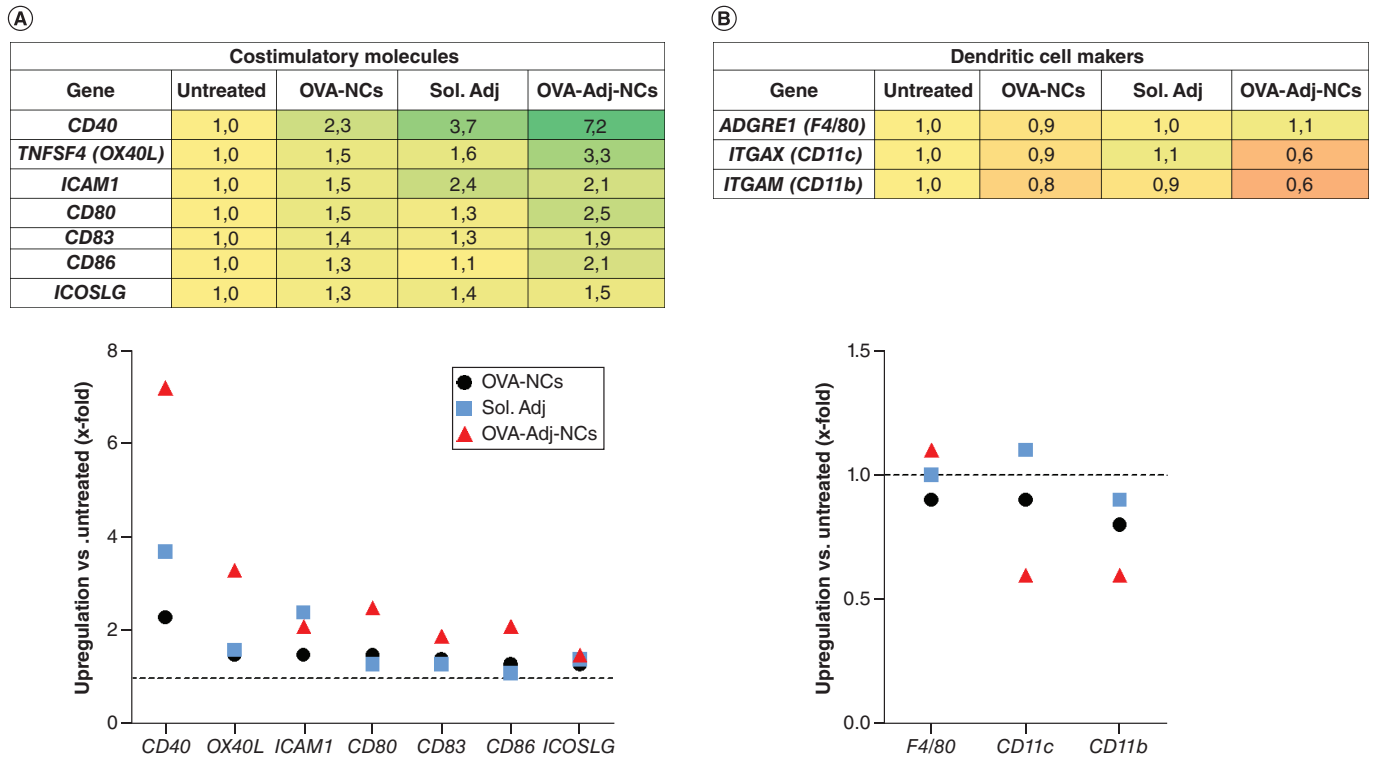


Figure 2. mRNA expression ratios of costimulatory molecules and dendritic cell markers. The relative mRNA expression ratios of (A) costimulatory molecules and (B) dendritic cell markers of bone marrow-derived dendritic cells (2×10^6 cells/ml) treated with empty OVA-NCs, OVA-Adj-NCs (both $75 \mu\text{g/ml}$), or equimolar amounts of soluble adjuvants were calculated against the untreated control. Dashed line indicates mRNA expression of untreated control. Tests were performed in duplicate ($n = 2$). NC: Nanocapsule; OVA: Ovalbumin.

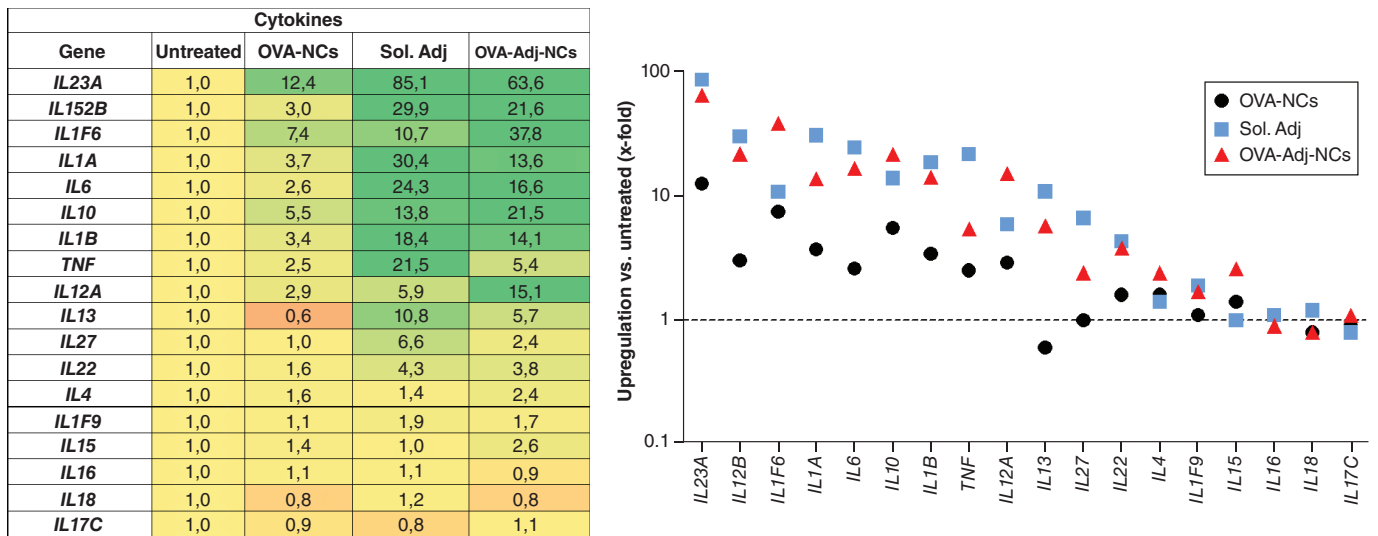


Figure 3. mRNA expression ratios of cytokines. The relative mRNA expression ratios of cytokines of bone marrow-derived dendritic cells (2×10^6 cells/ml) treated with empty OVA-NCs, OVA-Adj-NCs (both $75 \mu\text{g/ml}$), or equimolar amounts of soluble adjuvants were calculated against the untreated control. Y-axis is visualized in logarithmic scale. Dashed line indicates mRNA expression of untreated control. Tests were performed in duplicate ($n = 2$). NC: Nanocapsule; OVA: Ovalbumin.

CD11c [24] and *CD11b* [25] have been described to be associated with DC stimulation. Therefore, the results indicate a more extensive stimulation in case of encapsulated application compared with soluble.

Upregulation of cytokines is only slightly different between soluble & encapsulated adjuvants

Cytokines as an elemental component of every immune reaction were also analyzed by RNA-Seq. Cytokine mRNA expression analysis showed that empty OVA-NCs induced only a decent increase in the mRNA expression of *IL1A*, *IL6*, *IL12A*, *IL12B* and *TNF*, while the expression levels of *IL1F6*, *IL10*, and particularly *IL23A* were noticeably upregulated. The resulting IL-23 belongs to the pro-inflammatory IL-12 family and is known to support Th17 differentiation [26]. Compared with this, BMDC treatment with OVA-Adj-NCs as well as soluble adjuvants evoked a strong increase in the mRNA expression of numerous, but almost the same cytokines. In this regard, the soluble adjuvant treatment showed in many cases higher expression ratios than the OVA-Adj-NC treatment, for instance for *IL23A*, *IL1A* and *TNF*. Nonetheless, some cytokines, such as *IL12A* and *IL1F6*, were more upregulated by the encapsulated adjuvants. In comparison with the untreated control, both adjuvant treatments triggered specific, but comparable cytokine patterns (Figure 3). Again, the results agreed with previous ones showing increased secretion of IL-1 β , IL-6, TNF- α and IL-12 upon treatment with OVA-Adj-NCs. Particularly interesting was the strong upregulation of *IL12A* compared with the soluble adjuvant treatment, since it is necessary to form a functional IL-12. In contrast, the soluble adjuvants triggered higher amounts of *TNF* mRNA. Nonetheless, we have previously shown that OVA-Adj-NC-treated BMDC produce both IL-12 and TNF- α in high amounts [1]. Except *IL10* mRNA, which encodes for the anti-inflammatory IL-10, only pro-inflammatory cytokine mRNAs were upregulated upon stimulation with MDP + R848, whether soluble or encapsulated.

MHC appears to be slightly overexpressed for encapsulated adjuvants

Analysis of the relative mRNA expression ratios of different MHC-I and MHC-II molecules in BMDCs revealed an increased expression of some prominent MHC-I molecules, such as *H2-Q10* and *H2-Q4*, as well as of the MHC-I base component β 2 microglobulin (*B2M*) upon treatment with OVA-Adj-NCs compared with the untreated control. Even though a slight increase of those molecules was detectable after BMDC incubation with empty OVA-NC and soluble adjuvants, it was in both cases considerably weaker compared with the first-mentioned treatment. Regarding MHC-II molecules, only *H2-Eb2* mRNA was upregulated upon treatment with empty OVA-NCs and OVA-Adj-NCs. Application of soluble adjuvants did not show any effect in this context (Figure 4).

Up/downregulation of chemokine expression

Regarding chemokine mRNAs, we observed complex expression patterns induced by all three treatments compared with the untreated control. Thereby, numerous mRNAs were upregulated specifically by both adjuvant treatments, such as *CCL1*, *CXCL5* or *CCL4*, while *CXCL9*, *CXCL10* and *CCL1* mRNA expression was also stimulated by empty OVA-NCs. While the expression of the chemokines *CXCL1*, *CCL1* and *CXCL2* was more triggered by soluble MDP/R848, *CXCL9* and *CXCL10* mRNA expression was much more enhanced by OVA-Adj-NCs. This resulted in relative expression ratios of more than 50 compared with untreated cells (Figure 5).

Up/downregulation of other groups of genes

Besides these striking results, further gene groups revealed distinct effects triggered by OVA-Adj-NCs and the soluble adjuvant combination, respectively. Regarding TLRs/NLRs and scavenger receptors, increased amounts of *NLRP3*, *TLR2*, *TLR7* and *TLR8* mRNAs were detectable upon treatment with soluble MDP/R848 (Supplementary Figure 11), whereas the transcriptional expression of *CD14* and *MARCO* was enhanced by both (Supplementary Figure 11). While TLR and NLR expression highly depends on specific cell type and maturation state [27], CD14 as well as MARCO have already been described to be upregulated in DCs by successful stimulation [28,29]. In contrast, mRNA expression of the C-type lectin *LY75* (*DEC-205*), which is highly associated with the expression of CD8 α in lymphoid DCs [30], was upregulated (2.4-fold) in BMDCs, when they were treated with OVA-Adj-NCs but not with soluble adjuvants (Supplementary Figure 12). Another parameter to assess effective DC maturation is the expression profile of chemokine receptors. BMDC treatment with OVA-Adj-NCs evoked a transcriptional upregulation of *CXCR5* as well as *CCR7*. In contrast, the stimulation with soluble adjuvants did not change the mRNA expression of these two receptors at all. Empty OVA-NCs only triggered slight increases of both. At the same time, the mRNA expression of the chemokine receptors *CCR1*, *CCR2* and *CCR5* was downregulated by the adjuvant-loaded OVA-NCs but not by the soluble adjuvants (Supplementary Figure 13). Interestingly, an increased

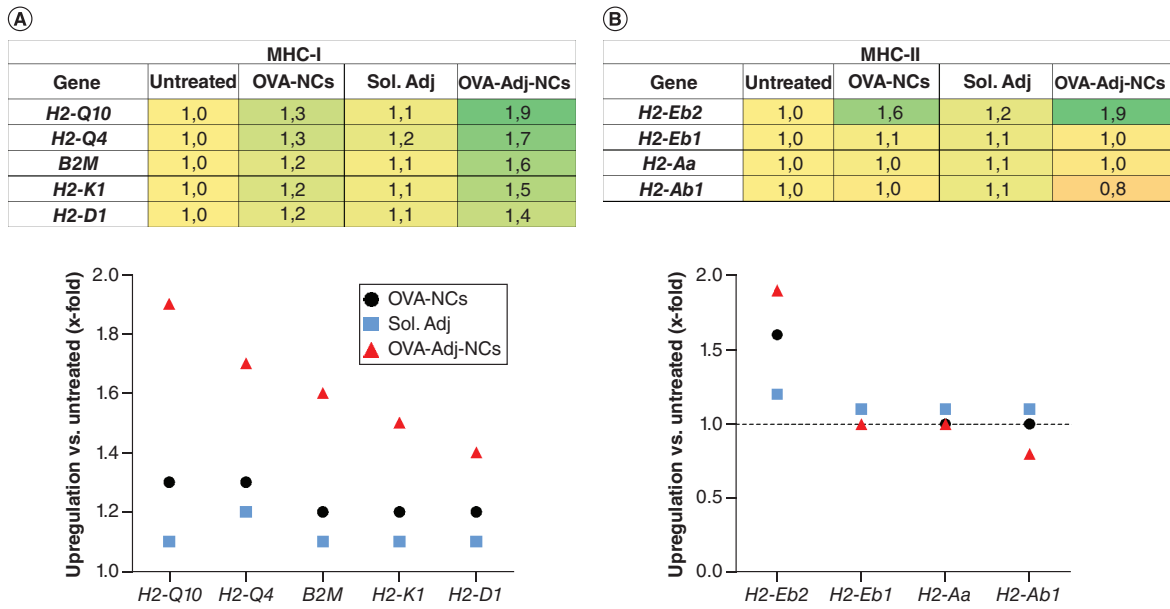


Figure 4. mRNA expression ratios of MHC-I/II molecules. The relative mRNA expression ratios of **(A) MHC-I** and **(B) MHC-II** molecules of bone marrow-derived dendritic cells (2×10^6 cells/ml) treated with empty OVA-NCs, OVA-Adj-NCs (both $75 \mu\text{g/ml}$) or equimolar amounts of soluble adjuvants were calculated against the untreated control. Dashed line indicates mRNA expression of untreated control. Tests were performed in duplicate ($n = 2$). NC: Nanocapsule; OVA: Ovalbumin.

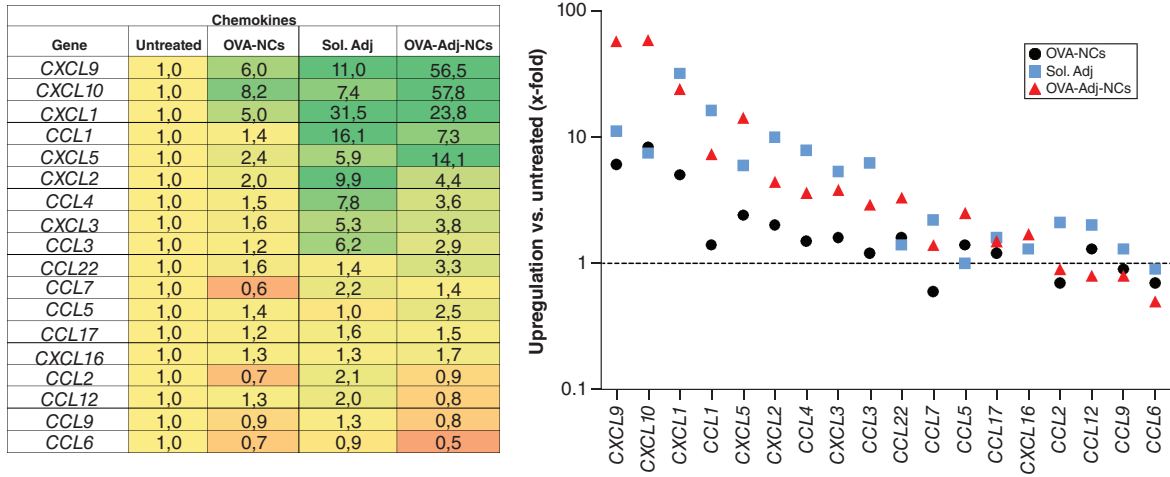


Figure 5. mRNA expression ratios of chemokines. The relative mRNA expression ratios of chemokines of bone marrow-derived dendritic cells (2×10^6 cells/ml) treated with empty OVA-NCs, OVA-Adj-NCs (both $75 \mu\text{g/ml}$) or equimolar amounts of soluble adjuvants were calculated against the untreated control. Y axis is visualized in logarithmic scale. Dashed line indicates mRNA expression of untreated control. Tests were performed in duplicate ($n = 2$). NC: Nanocapsule; OVA: Ovalbumin.

expression of CXCR5 and CCR7 combined with decreased amounts of CCR1, CCR2 and CCR5 has been defined by Oppenheim *et al.* as characteristics of fully-matured DCs [31,32]. The transcriptional chemokine receptor profile of OVA-Adj-NC-treated BMDCs closely matched these specifications, while those treated with soluble adjuvants or empty OVA-NCs did not. As an internal control, the mRNAs of 19 housekeeping genes were measured. As expected, no transcriptional alterations were detectable for the different treatments (Supplementary Figure 14).

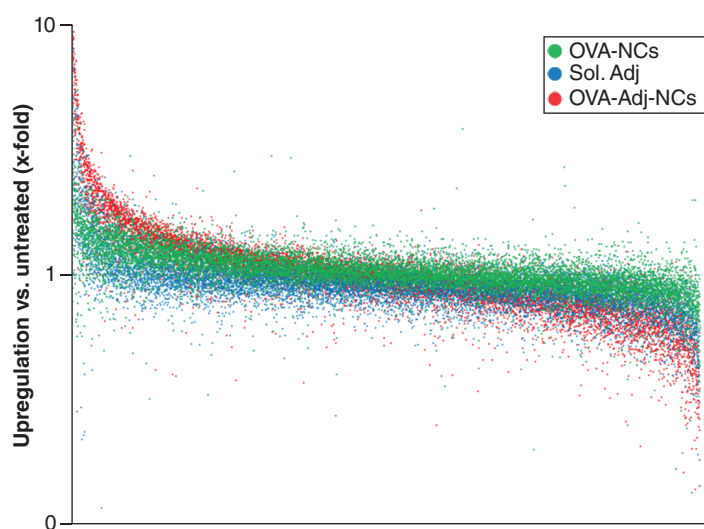


Figure 6. Relative transcriptome changes of differently treated bone marrow-derived dendritic cells versus untreated control. Mean values of the two biological replicates were calculated and the relative expression ratios of bone marrow-derived dendritic cells (2×10^6 cells/ml) treated with either empty OVA-NCs, muramyl dipeptide/resiquimod-loaded OVA-NCs (both $75 \mu\text{g/ml}$) or equimolar amounts of soluble muramyl dipeptide/resiquimod ($287.25 \text{ ng/ml}/83.25 \text{ ng/ml}$) against the untreated control were determined for each gene. Y-axis is visualized in logarithmic scale. Each dot represents one gene. Tests were performed in duplicate ($n = 2$). NC: Nanocapsule; OVA: Ovalbumin.

Overall gene expression upon treatment

The overall increase in gene expression was analyzed with a threshold factor of at least 1.5. Under these rules, the expression of 418 genes was identified to be increased after treatment with soluble MDP/R848. The treatment with the empty OVA-NCs resulted in an upregulation of 518 genes. Interestingly, the combination of both, meaning MDP/R848-loaded OVA-NCs, triggered an increase of 1225 genes. The same tendency was observed for transcriptomic downregulation upon treatment (threshold factor of at least 0.5). Cells treated with soluble MDP/R848 revealed 161 downregulated genes, whereas cells treated with empty OVA-NCs showed 45 downregulated genes. In contrast, the expression of 478 genes was identified to be decreased after treatment with MDP/R848-loaded OVA-NCs. All changes in the transcriptome of differently treated cells compared with the untreated control were visualized in a graph (Figure 6). Significantly more genes were upregulated or downregulated upon treatment with MDP/R848-loaded OVA-NCs than with the soluble equivalents or empty OVA-NCs. Furthermore, many genes showed a much stronger increase in expression in this sample.

RNA-Seq versus qPCR

Compared with the widely used Sanger sequencing, NGS methods (such as RNA-Seq) as well as qPCR provide significantly higher but similar analytical sensitivity, specificity and high concordance [33]. To confirm the RNA-Seq results with an additional method, we picked representative upregulated (*IL12B*, *IRF7*, *CXCL10* and *NOS2*) and downregulated (*F2RL2*) as well as only slightly influenced genes (*CD11c* and *HSPA8*) and determined the relative gene expression levels by qPCR. The calculated relative copy numbers (untreated was set as 1) of all measured upregulated genes revealed similar tendencies for the two methodologies. In case of *IL12B*, the relative copy numbers were almost the same, whereas for *IRF7* and *CXCL10* qPCR results showed higher expressions. In contrast, the copy numbers for *NOS2* were lower for qPCR (Figure 7). A comparison of the relative copy numbers of the mentioned downregulated and slightly influenced genes via RNA-Seq and qPCR exposed a high level of agreement for the two result groups. *F2RL2*, *CD11c* as well as *HSPA8* showed comparable copy numbers (Supplementary Figure 15). Our qPCR results confirmed those of RNA-Seq. Although the relative copy numbers were not completely comparable, the general progressions measured by qPCR strongly correlated with those of RNA-Seq.

Quantitative proteomic analysis

As a complementary approach to our transcriptome analysis, we performed a comprehensive proteomic analysis of the cellular proteome after NC and soluble adjuvant treatment. In parallel to the RNA extraction (as described above), intracellular proteins were extracted, digested and analyzed via label free high-resolution mass spectrometry. The absolute amount of each protein in fmol was determined via the TOP/Hi3 approach [18]. We further calculated the relative ratio of each protein in the treated sample versus untreated cells. All proteins, which were enriched more than two-times, were classified into eight different protein classes based on their biological function (Figure 8A) and their relative amount in percent was calculated.

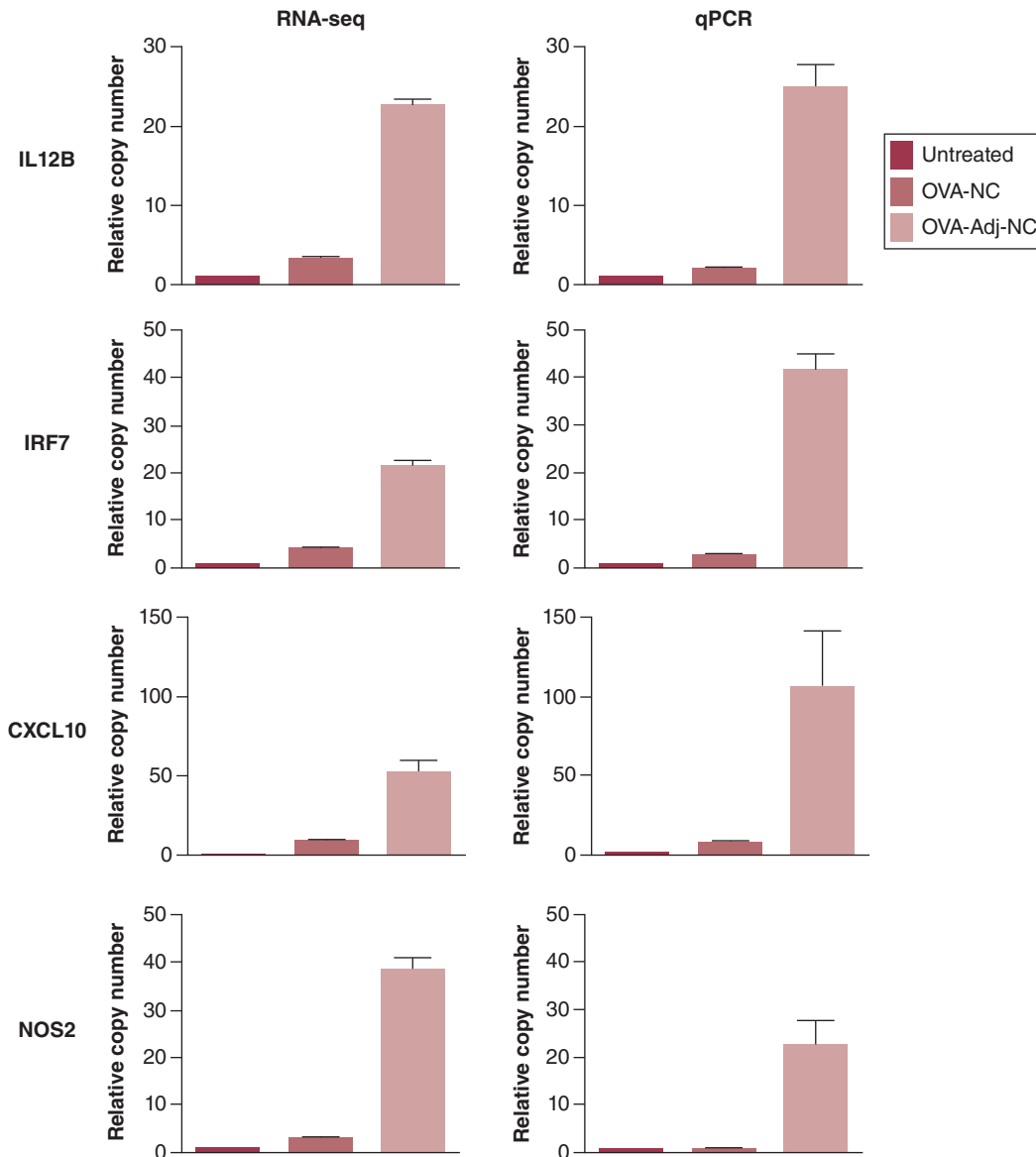


Figure 7. Comparison of upregulated genes determined by RNA-Seq and qPCR. To verify the RNA-Seq results via qPCR, bone marrow-derived dendritic cells (2×10^6 cells/ml) were treated with empty OVA-NCs or OVA-Adj-NCs (both $75 \mu\text{g/ml}$). The relative mRNA copy numbers of four representative upregulated genes (*IL12B*, *IRF7*, *CXCL10* and *NOS2*) were measured by RNA-Seq and qPCR, and plotted comparatively against the untreated control. NC: Nanocapsule; OVA: Ovalbumin.

Here, we found that there was a significant difference in the cellular proteome after NC treatment in comparison with the soluble adjuvants. Proteins involved in the trafficking process and signal transduction are highly enriched in the cellular proteome after NCs treatment in comparison with the soluble adjuvants. In contrast, we detected a significant higher amount of cellular proteins involved in the immune response after treatment with the soluble adjuvants in comparison with the encapsulated ones. A full list of all identified proteins is additionally provided in a separate Excel sheet.

For a deeper proteomic analysis, a hierarchical cluster analysis was carried out using the web tool ClustVis (Figure 8B). Most strikingly, we saw that Ras-related proteins or granulins were significantly enriched after NC treatment. All of these proteins are involved in intracellular membrane trafficking process and endosomal transport [13]. Therefore, these data give insight into the cellular uptake processes of the NCs.

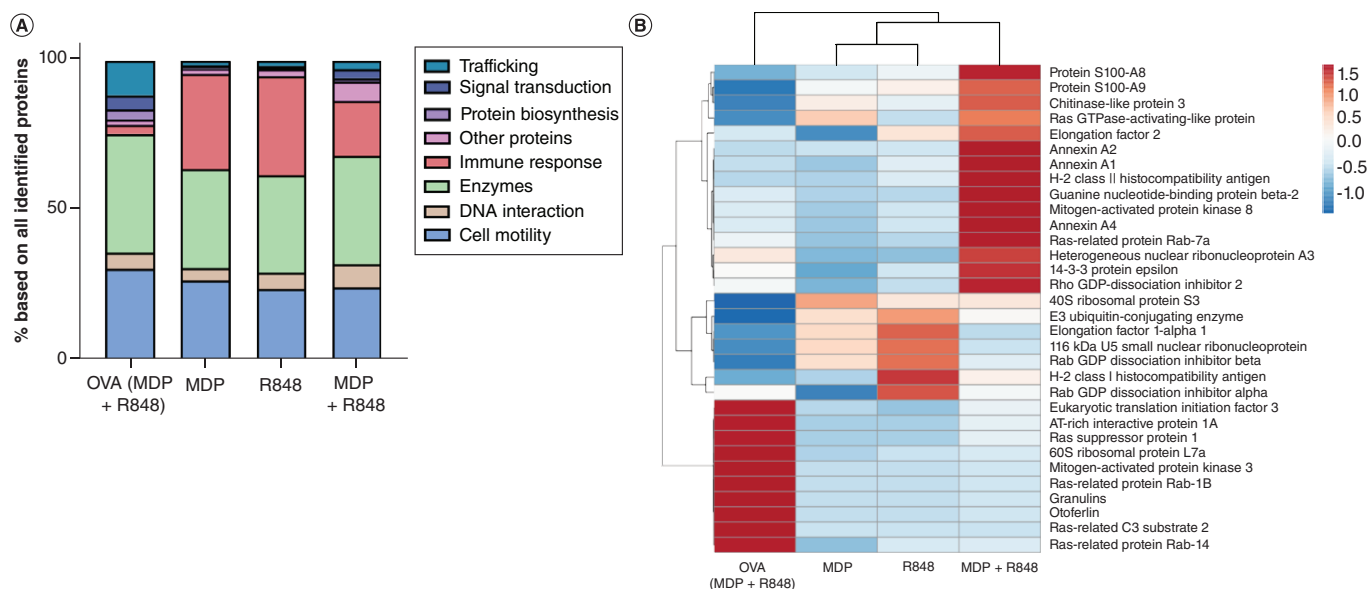


Figure 8. Analysis of intracellular proteins. Protein classification (A) and hierarchical clustering analysis (B). Bone marrow-derived dendritic cells (2×10^6 cells/ml) were treated with OVA-Adj-NCs (75 $\mu\text{g/ml}$) or equimolar amounts of soluble adjuvants. Cellular proteins were extracted, analyzed by label-free shotgun proteomics and classified into eight different classes based on their biological Proteins, which are enriched more than two-times, were analyzed with the web tool ClustVis. Tests are performed from a duplicate dataset ($n = 2$). MDP: Muramyl dipeptide; NC: Nanocapsule; OVA: Ovalbumin; R848: Resiquimod.

In contrast, after treatment with the soluble adjuvant combination, cellular proteins involved in the immune response, for example protein S100-A8/A9 or H-2 class II histocompatibility antigen were upregulated. Most interestingly, there was a prominent difference for cells treated with the single adjuvants versus the combined adjuvants underlining the synergistic effect a specific adjuvant combination. Hence, the strong immunological response of the encapsulated adjuvant combination was not observed on a protein level. However, for the presented experiments the incubation time ranged from 1 to 4 h. Therefore, the lower immunological response of the NCs in comparison with the soluble adjuvants could be caused by differences in the cellular uptake kinetics and intracellular processing.

Discussion

Demonstrating the effect of adjuvant loaded nanocarriers can be done in a targeted fashion, in other words, looking at the expression level of selected genes. This is usually done by picking important genes as they have been reported in literature to be influenced by the specific adjuvant. Unfortunately, this approach is blind toward effects of adjuvants delivery by nanocarriers and how they enable a better stimulation of some pathways of intracellular and extracellular signaling. We have demonstrated that a NGS approach gives a clearer and is able to provide an all-embracing approach. Hereby, a quantitative comparison between encapsulated and nonencapsulated adjuvants can be achieved.

For all formulations tested, ISGs played a prominent role in our analysis and were highly upregulated for the encapsulated adjuvants versus the soluble ones. This is an extremely important result as ISGs play a major role in the immune response. ISGs, such as *RSAD2* (33, five-times overexpressed by adjuvant-loaded NCs) and *ISG15* (27-times overexpressed by adjuvant-loaded NCs), are especially attributed with an emerging role in antiviral immunity [34,35]. Moreover, both ISGs have already been described to be beneficial for an effective antitumor immune response which is important for other projects in the field of antitumor vaccination. *RSAD2* has been reported as a necessary factor for DC maturation in a B16F10 pulmonary metastasis model [22], while *ISG15* has been identified to trigger antitumor immune responses by promoting intratumoral infiltration of NK cells and enhancing antigen presentation in tumor cells [36]. Moreover, Bidwell *et al.* have identified *IRF7* silencing to promote metastasis in breast cancer [37]. Since ISG expression is defined as a first line of host defense against virus infections [21], it seems that only the combined application of antigen and adjuvant mimics the presence of a potential virus-like thread sufficiently in this setup, whereas antigen-NC or superadditive adjuvant combination

alone fail. Although the transcriptome profiles were striking, the absence of a soluble antigen-only control in RNA expression levels might be seen as a limitation for our data and should be addressed in future experiments.

It has already been reported by numerous studies that DC stimulation with adjuvants does not only evoke an increase of costimulatory molecules on protein level but also a transcriptional upregulation [38–40]. Since costimulatory molecules are highly essential for the induction of DC-mediated T-cell activation [41], increased amounts of such mRNAs are advantageous if you strive for a strong T-cell response. Our results demonstrate that a nanocapsular packaging device supports the enhanced intracellular delivery of MDP and R848 toward their endosomal (TLR7 for R848) or cytoplasmic (NOD2 for MDP) target especially by enhancing the upregulation of CD40, but also classical markers like CD80, CD83 and CD86 and that nanoencapsulated adjuvants yield a higher costimulatory effect.

Besides the cell surface markers of costimulation, we investigated the upregulation of cytokines. Here, we found high upregulation of *IL23A* and *IL12*, but with no clear advantage for the nanoencapsulated form. Nevertheless, cytokines are the most important secondary signal for an efficient vaccination response. IL-12 is the key mediator of Th1 differentiation, which is highly desirable in tumor vaccination, whereas TNF is controversially discussed regarding its pro and antitumoral effects [42]. Consequently, IL-12 is of more relevance in this study. It has been reported by several studies that DC stimulation with different adjuvants not only triggers increased secretion of proinflammatory cytokines but also an upregulation of those markers, particularly TNF- α , IL-1 β and IL-6, on transcriptional level [38–40]. Moreover, Hotz *et al.* reported in 2016 that BMDC stimulation with R848 for 4 h triggered increased mRNA expression of *IL6*, *IL12A* and *IL12B* [5]. IL-10, a major suppressive cytokine, is known to inhibit MHC-II and CD80/CD86 expression as well as the production of proinflammatory cytokines in DCs [43]. Furthermore, autocrine IL-10 signaling can block IL-12 production [44]. Due to the underlying negative feedback loop (IL-12 production triggers IL-10) and the result that the mRNAs of the IL-12 subunits IL-12p35 (*IL12A*) and IL-12p40 (*IL12B*) were also upregulated, it was expected to detect elevated levels of IL-10. Interestingly, there are some cytokines which show a higher relative transcriptional expression upon treatment with the soluble adjuvants (such as *IL1A* and *TNF*) compared with the encapsulated. A possible explanation is that TNF as well as *IL1A* encode cytokines which belong to the early stage cytokines, so cytokines which are secreted early in case of an immune reaction. Since the soluble adjuvants are much earlier available for receptor binding (and thus stimulation) upon cellular uptake compared with the encapsulated ones (intracellular release required), it is likely that they induce the transcriptional upregulation of such early stage cytokines earlier. In general, the transcriptional expression pattern of cytokines upon stimulation over time is a very complex issue. It highly depends on the maturation stage of the DCs. In total, both the soluble and the encapsulated combination of MDP + R848 triggered strong and highly similar proinflammatory mRNA cytokine profiles, despite the fact that OVA-NCs have to be degraded first.

Antigen presentation via MHC-I is essential for the induction of cytotoxic T-cell responses, which are important for an effective tumor fighting. Therefore, an increased expression of according mRNAs might enhance such responses and result in a better outcome. Most importantly, the nanoencapsulated adjuvants showed here some effect while the soluble adjuvants did not. As in case of ISGs, also MHC-I-coding genes seem to require both antigen and adjuvant for a sufficient transcription.

Chemokines in general are responsible for chemotaxis, cell differentiation and the recruitment of specific immune cells. Here also found striking effects for the nanoencapsulated adjuvants in comparison with the soluble ones. In particular, *CXCL9* and *CXCL10* have been reported to be positively associated with tumor suppression [45] and are, thereby, recognized by the same receptors, namely CXCR3, which is mainly expressed on Th1 T cells and NK cells upon activation. Furthermore, they have both been described as essential factors inducing the recruitment and infiltration of tumor-suppressive CXCR3⁺ T cells and NK cells into solid tumors [46–48]. Consequently, an increased expression of *CXCL9* and *CXCL10* mRNA by DCs as demonstrated by our results for nanoencapsulated adjuvants might be promising for potential tumor vaccinations with MDP/R848-loaded protein NCs and may contribute to a better performance of a nanoencapsulated vaccine with adjuvants.

Besides these groups of genes overexpressed after administration of adjuvants or even better nanoencapsulated adjuvants, we observed the upregulation of gene expression which were standing alone. For example, DEC-205 was observed to be upregulated in our study. Butler *et al.* reported in 2007 that DEC-205 is upregulated upon effective DC maturation by molecule redistribution and *de novo* synthesis [49]. In the group of IFN signaling-associated genes, the mRNA expression of the mentioned *IRF7* but also *STAT1*, *STAT2*, and to a certain extent *IRF1*, *IRF9* and *IRF8* was stimulated more effectively by OVA-Adj-NCs than by the soluble adjuvants or empty OVA-NCs (Supplementary Figure 10). STAT1 and STAT2 are key mediators of Type I and III IFN signaling, therefore

important for cellular antiviral responses and the mediation of adaptive immunity [50]. Thereby, they interact with IRF9 to form the transcription factor ISGF3, which mediates the transcription of numerous ISGs [51]. IRF1 and IRF8 work in a similar way by binding and triggering IFN stimulated response element promoters in the nucleus, leading to ISG expression [52,53]. In this regard, the transcriptional upregulation of those essential regulatory IFN signaling-associated genes upon treatment with OVA-Adj-NCs provides a clear explanation for the massive ISG mRNA expression.

Conclusion

Altogether, our study demonstrated the induction of numerous immunologically relevant molecules on mRNA level in BMDCs upon treatment with MDP/R848-loaded OVA-NCs. Thereby, the combined application of antigen and adjuvant in one nanocarrier triggered a much broader transcriptional response compared with a treatment with equimolar amounts of soluble MDP/R848 or empty OVA-NCs. In particular, the IFN signaling pathway associated with ISG expression was massively influenced by the adjuvant-loaded NCs, whereas single application of OVA-NC and adjuvants, respectively, did not. Interestingly, Type I IFN mRNA (e.g., *IFNA1* and *IFNB1*) was not detectable in any case, though some of their known repressors, such as *SOCS3* [54] or *PRDMI* [55], showed an increased transcriptional expression in the presence of adjuvants. It is known that Type I IFNs underlie a rapid transcriptional decrease upon induction due to transcriptional repression and mRNA turnover [56]. Moreover, Abe *et al.* have reported transient increases and decreases in IFN- β mRNA expression after adjuvant stimulation [57]. We concluded that the delivery of both antigen-NCs and adjuvants was much more efficient in inducing a strong activation of IFN signaling in this setup, which in turn triggered an increased expression of various ISGs. Since neither antigen-NCs nor adjuvants alone did so, this effect can only be attributed to the combination of both in one system. Considering that several ISGs have been described to show antiviral or even antitumor activity, this might be an important aspect to take into account in future nanovaccine approaches.

Summary points

- The immune response of bone marrow-derived dendritic cell treated with an adjuvant combination resiquimod and muramyl dipeptide in a soluble form versus encapsulated into a nanocarrier was studied by next-generation sequencing.
- A total of 1225 genes were upregulated after nanocarrier treatment, while 478 genes were downregulated in bone marrow-derived dendritic cells.
- The combined application of antigen and adjuvant in a nanocarrier triggered a much stronger and broad transcriptional response compared with a treatment with soluble adjuvants.
- The expression of interferon-stimulated genes was heavily influenced by the adjuvant-loaded nanocapsules (NC) in comparison with soluble adjuvants or ovalbumin (OVA)-NCs without adjuvants.
- IL-12A and MHC-I and -II were stronger expressed for the encapsulated form while this was not the case for the soluble application.
- The next-generation sequencing data were verified by qPCR for selected genes.
- The combined application of antigen and adjuvant in a nanocarrier triggered a much broader transcriptional response compared with a treatment with equimolar amounts of soluble adjuvants or OVA-NCs only.
- The cellular uptake pathway of the nanocarriers of OVA nanocarriers was additionally studied by label-free shotgun proteomics.
- A comprehensive overview about immunological properties of nanocarriers used for vaccination is presented to evaluate their *in vivo* efficacy.

Supplementary data

To view the supplementary data that accompany this paper please visit the journal article at: www.futuremedicine.com/doi/suppl/10.2217/nnm-2019-0460

Financial & competing interests disclosure

This work was supported by a personal grant of the Max-Planck-Graduate Center, Mainz (MPGC) to D Paßlick and was also supported by the Deutsche Forschungsgemeinschaft in the CRC1066 "Collaborative Research Center 1066: Nanodimensional polymer therapeutics for tumor therapy". The authors have no other relevant affiliations or financial involvement with any organization or entity with a financial interest in or financial conflict with the subject matter or materials discussed in the manuscript apart from those disclosed.

No writing assistance was utilized in the production of this manuscript.

Ethical conduct of research

The authors state that they have obtained appropriate institutional review board approval or have followed the principles outlined in the Declaration of Helsinki for all human or animal experimental investigations.

Open access

This work is licensed under the Attribution-NonCommercial-NoDerivatives 4.0 Unported License. To view a copy of this license, visit <http://creativecommons.org/licenses/by-nc-nd/4.0/>

References

1. Passlick D, Piradashvili K, Bamberger D *et al.* Delivering all in one: antigen-nanocapsule loaded with dual adjuvant yields superadditive effects by DC-directed T cell stimulation. *J. Control. Rel.* 289, 23–34 (2018).
2. Piradashvili K, Fichter M, Mohr K, Gehring S, Wurm FR, Landfester K. Biodegradable protein nanocontainers. *Biomacromolecules* 16(3), 815–821 (2015).
3. Mathan TSM, Textor J, Skold AE *et al.* Harnessing RNA sequencing for global, unbiased evaluation of two new adjuvants for dendritic-cell immunotherapy. *Oncotarget* 8(12), 19879–19893 (2017).
4. Wu M, Wang H, Shi J *et al.* Gene expression profiles identify both MyD88-independent and MyD88-dependent pathways involved in the maturation of dendritic cells mediated by heparan sulfate: a novel adjuvant. *Hum. Vaccin. Immunother.* 10(12), 3711–3721 (2014).
5. Hotz C, Treinies M, Mottas I *et al.* Reprogramming of TLR7 signaling enhances anti-tumor NK and cytotoxic T cell responses. *Oncoimmunology* 5(11), e1232219 (2016).
6. Costa V, Righelli D, Russo F, De Berardinis P, Angelini C, D'apice L. Distinct antigen delivery systems induce dendritic cells' divergent transcriptional response: new insights from a comparative and reproducible computational analysis. *Int. J. Mol. Sci.* 18(3), (2017).
7. Helft J, Bottcher J, Chakravarty P *et al.* GM-CSF Mouse bone marrow cultures comprise a heterogeneous population of CD11c(+)MHCII(+) macrophages and dendritic cells. *Immunity* 42(6), 1197–1211 (2015).
8. Van Goor A, Slawinska A, Schmidt CJ, Lamont SJ. Distinct functional responses to stressors of bone marrow derived dendritic cells from diverse inbred chicken lines. *Dev. Comp. Immunol.* 63, 96–110 (2016).
9. Schlaad H, Kukulka H, Rudloff J, Below I. Synthesis of α,ω -heterobifunctional poly(ethylene glycol)s by metal-free anionic ring-opening polymerization. *Macromolecules* 34(13), 4302–4304 (2001).
10. Bros M, Montermann E, Cholaszczynska A, Reske-Kunz AB. The phosphodiesterase 4 inhibitor roflumilast augments the Th17-promoting capability of dendritic cells by enhancing IL-23 production, and impairs their T cell stimulatory activity due to elevated IL-10. *Int. Immunopharmacol.* 35, 174–184 (2016).
11. Zal T, Volkman A, Stockinger B. Mechanisms of tolerance induction in major histocompatibility complex class II-restricted T cells specific for a blood-borne self-antigen. *J. Exp. Med.* 180(6), 2089–2099 (1994).
12. Livak KJ, Schmittgen TD. Analysis of relative gene expression data using real-time quantitative PCR and the 2(-Delta Delta C(T)) method. *Methods* 25(4), 402–408 (2001).
13. Hofmann D, Tenzer S, Bannwarth MB *et al.* Mass spectrometry and imaging analysis of nanoparticle-containing vesicles provide a mechanistic insight into cellular trafficking. *ACS Nano* 8(10), 10077–10088 (2014).
14. Tenzer S. Nanoparticle size is a critical physicochemical determinant of the human blood plasma corona: a comprehensive quantitative proteomic analysis. *ACS Nano* 5, 7155–7167 (2011).
15. Bradshaw RA, Burlingame AL, Carr S, Aebersold R. Reporting protein identification data: the next generation of guidelines. *Mol. Cell. Proteomics* 5(5), 787–788 (2006).
16. Müller LK, Simon J, Schöttler S, Landfester K, Mailänder V, Mohr K. Pre-coating with protein fractions inhibits nano-carrier aggregation in human blood plasma. *RSC Adv.* 6(99), 96495–96509 (2016).
17. Simon J, Muller J, Ghazaryan A, Morsbach S, Mailänder V, Landfester K. Protein denaturation caused by heat inactivation detrimentally affects biomolecular corona formation and cellular uptake. *Nanoscale* 10(45), 21096–21105 (2018).
18. Silva JC, Gorenstein MV, Li GZ, Vissers JPC, Geromanos SJ. Absolute quantification of proteins by LCMSE: a virtue of parallel MS acquisition. *Mol. Cell. Proteomics* 5, 144–156 (2006).
19. Schroeder A, Mueller O, Stocker S *et al.* The RIN: an RNA integrity number for assigning integrity values to RNA measurements. *BMC Mol. Biol.* 7, 3 (2006).
20. Bult CJ, Eppig JT, Blake JA, Kadin JA, Richardson JE. The Mouse Genome Database Group. Mouse genome database 2016. *Nucleic Acids Res.* 44(Database issue), D840–D847 (2016).
21. Schoggins JW, Rice CM. Interferon-stimulated genes and their antiviral effector functions. *Curr. Opin. Virol.* 1(6), 519–525 (2011).
22. Jang JS, Lee JH, Jung NC *et al.* Rsad2 is necessary for mouse dendritic cell maturation via the IRF7-mediated signaling pathway. *Cell Death Dis.* 9(8), 823–823 (2018).
23. Ning S, Pagano JS, Barber GN. IRF7: activation, regulation, modification and function. *Genes Immunity* 12, 399 (2011).

24. Singh-Jasuja H, Thiolat A, Ribon M *et al.* The mouse dendritic cell marker CD11c is down-regulated upon cell activation through Toll-like receptor triggering. *Immunobiology* 218(1), 28–39 (2013).
25. Griffiths KL, Tan JKH, O'Neill HC. Characterization of the effect of LPS on dendritic cell subset discrimination in spleen. *J. Cell. Mol. Med.* 18(9), 1908–1912 (2014).
26. Park H, Li Z, Yang XO *et al.* A distinct lineage of CD4 T cells regulates tissue inflammation by producing interleukin 17. *Nat. Immunol.* 6, 1133 (2005).
27. Muzio M, Bosisio D, Polentarutti N *et al.* Differential expression and regulation of toll-like receptors (TLR) in human leukocytes: selective expression of TLR3 in dendritic cells. *J. Immunol.* 164(11), 5998–6004 (2000).
28. Mahnke K, Becher E, Ricciardi-Castagnoli P, Luger TA, Schwarz T, Grabbe S. CD14 is expressed by subsets of murine dendritic cells and upregulated by lipopolysaccharide. *Adv. Exp. Med. Biol.* 417, 145–159 (1997).
29. Kissick HT, Dunn LK, Ghosh S, Nechama M, Kobzik L, Arredouani MS. The scavenger receptor MARCO modulates TLR-induced responses in dendritic cells. *PLoS ONE* 9(8), e104148 (2014).
30. Idoyaga J, Suda N, Suda K, Park CG, Steinman RM. Antibody to Langerin/CD207 localizes large numbers of CD8alpha+ dendritic cells to the marginal zone of mouse spleen. *Proc. Natl Acad. Sci. USA* 106(5), 1524–1529 (2009).
31. Oppenheim JJ, Yang D, Biragyn A, Howard OZ, Plotz P. Chemokine receptors on dendritic cells promote autoimmune reactions. *Arthritis Res. Ther.* 4(3), S183 (2002).
32. Sallusto F, Palermo B, Lenig D *et al.* Distinct patterns and kinetics of chemokine production regulate dendritic cell function. *Eur. J. Immunol.* 29(5), 1617–1625 (1999).
33. Gao J, Wu H, Shi X, Huo Z, Zhang J, Liang Z. Comparison of next-generation sequencing, quantitative PCR, and Sanger sequencing for mutation profiling of EGFR, KRAS, PIK3CA and BRAF in clinical lung tumors. *Clin. Lab.* 62(4), 689–696 (2016).
34. Helbig KJ, Beard MR. The role of viperin in the innate antiviral response. *J. Mol. Biol.* 426(6), 1210–1219 (2014).
35. Skaug B, Chen ZJ. Emerging role of ISG15 in antiviral immunity. *Cell* 143(2), 187–190 (2010).
36. Burks J, Reed RE, Desai SD. Free ISG15 triggers an antitumor immune response against breast cancer: a new perspective. *Oncotarget* 6(9), 7221–7231 (2015).
37. Bidwell BN, Slaney CY, Withana NP *et al.* Silencing of *Irf7* pathways in breast cancer cells promotes bone metastasis through immune escape. *Nat. Med.* 18, 1224 (2012).
38. Ten Brinke A, Karsten ML, Dieker MC, Zwaginga JJ, Van Ham SM. The clinical grade maturation cocktail monophosphoryl lipid A plus IFNgamma generates monocyte-derived dendritic cells with the capacity to migrate and induce Th1 polarization. *Vaccine* 25(41), 7145–7152 (2007).
39. Massa C, Thomas C, Wang E, Marincola F, Seliger B. Different maturation cocktails provide dendritic cells with different chemoattractive properties. *J. Transl. Med.* 13, 175 (2015).
40. Zhu M, Xu W, Su H, Huang Q, Wang B. Addition of CpG ODN and Poly (I:C) to a standard maturation cocktail generates monocyte-derived dendritic cells and induces a potent Th1 polarization with migratory capacity. *Hum. Vaccin. Immunother.* 11(7), 1596–1605 (2015).
41. Corthay A. A three-cell model for activation of naive T helper cells. *Scand. J. Immunol.* 64(2), 93–96 (2006).
42. Wajant H. The role of TNF in cancer. *Results Probl. Cell Differ.* 49, 1–15 (2009).
43. Moore KW, De Waal Malefyt R, Coffman RL, O'Garra A. Interleukin-10 and the interleukin-10 receptor. *Annu. Rev. Immunol.* 19, 683–765 (2001).
44. Demangel C, Bertolino P, Britton WJ. Autocrine IL-10 impairs dendritic cell (DC)-derived immune responses to mycobacterial infection by suppressing DC trafficking to draining lymph nodes and local IL-12 production. *Eur. J. Immunol.* 32(4), 994–1002 (2002).
45. Tokunaga R, Zhang W, Naseem M *et al.* CXCL9, CXCL10, CXCL11/CXCR3 axis for immune activation – a target for novel cancer therapy. *Cancer Treat. Rev.* 63, 40–47 (2018).
46. Yang X, Chu Y, Wang Y, Zhang R, Xiong S. Targeted *in vivo* expression of IFN-gamma-inducible protein 10 induces specific antitumor activity. *J. Leukoc. Biol.* 80(6), 1434–1444 (2006).
47. Gorbachev AV, Kobayashi H, Kudo D *et al.* CXC chemokine ligand 9/monokine induced by IFN-gamma production by tumor cells is critical for T cell-mediated suppression of cutaneous tumors. *J. Immunol.* 178(4), 2278–2286 (2007).
48. Wendel M, Galani IE, Suri-Payer E, Cerwenka A. Natural killer cell accumulation in tumors is dependent on IFN-gamma and CXCR3 ligands. *Cancer Res.* 68(20), 8437–8445 (2008).
49. Butler M, Morel A-S, Jordan WJ *et al.* Altered expression and endocytic function of CD205 in human dendritic cells, and detection of a CD205–DCL-1 fusion protein upon dendritic cell maturation. *Immunology* 120(3), 362–371 (2007).
50. Au-Yeung N, Mandhana R, Horvath CM. Transcriptional regulation by STAT1 and STAT2 in the interferon JAK-STAT pathway. *JAK-STAT* 2(3), e23931–e23931 (2013).
51. Platanius LC. Mechanisms of type-I- and type-II-interferon-mediated signalling. *Nat. Rev. Immunol.* 5(5), 375–386 (2005).

52. Hu Y, Park-Min K-H, Yarilina A, Ivashkiv LB. Regulation of STAT pathways and IRF1 during human dendritic cell maturation by TNF-alpha and PGE2. *J. Leukoc. Biol.* 84(5), 1353–1360 (2008).
53. Aliberti J, Schulz O, Pennington DJ *et al.* Essential role for ICSBP in the *in vivo* development of murine CD8alpha + dendritic cells. *Blood* 101(1), 305–310 (2003).
54. Yu CF, Peng WM, Schlee M *et al.* SOCS1 and SOCS3 target IRF7 degradation to suppress TLR7-mediated Type I IFN production of human plasmacytoid dendritic cells. *J. Immunol.* 200(12), 4024–4035 (2018).
55. Ren B, Chee KJ, Kim TH, Maniatis T. PRDI-BF1/Blimp-1 repression is mediated by corepressors of the Groucho family of proteins. *Genes Dev.* 13(1), 125–137 (1999).
56. Whittemore LA, Maniatis T. Postinduction turnoff of beta-interferon gene expression. *Mol. Cell. Biol.* 10(4), 1329–1337 (1990).
57. Abe K, Ishigami T, Shyu A-B, Ohno S, Umemura S, Yamashita A. Analysis of interferon-beta mRNA stability control after poly(I:C) stimulation using RNA metabolic labeling by ethynyluridine. *Biochem. Biophys. Res. Comm.* 428(1), 44–49 (2012).